PCCP

Cite this: *Phys. Chem. Chem. Phys.*, 2011, **13**, 19471–19479

www.rsc.org/pccp

PAPER

^{95}Mo nuclear magnetic resonance parameters of molybdenum hexacarbonyl from density functional theory: appraisal of computational and geometrical parameters†

Jérôme Cuny,‡[a] Kateryna Sykina,[a] Bruno Fontaine,[a] Laurent Le Pollès,[a] Chris J. Pickard[b] and Régis Gautier*[a]

Received 13th July 2011, Accepted 7th September 2011
DOI: 10.1039/c1cp22289a

Solid-state ^{95}Mo nuclear magnetic resonance (NMR) properties of molybdenum hexacarbonyl have been computed using density functional theory (DFT) based methods. Both quadrupolar coupling and chemical shift parameters were evaluated and compared with parameters of high precision determined using single-crystal ^{95}Mo NMR experiments. Within a molecular approach, the effects of major computational parameters, *i.e.* basis set, exchange–correlation functional, treatment of relativity, have been evaluated. Except for the isotropic parameter of both chemical shift and chemical shielding, computed NMR parameters are more sensitive to geometrical variations than computational details. Relativistic effects do not play a crucial part in the calculations of such parameters for the 4d transition metal, in particular isotropic chemical shift. Periodic DFT calculations were tackled to measure the influence of neighbouring molecules on the crystal structure. These effects have to be taken into account to compute accurate solid-state ^{95}Mo NMR parameters even for such an inorganic molecular compound.

1 Introduction

In the field of transition metal (TM) computational chemistry, relativistic effects can play an important part, especially for the heaviest elements. The concept of heavy atoms is not univocal in the field of quantum modeling, the need for a relativistic theoretical treatment of chemical systems depends upon the desired level of accuracy as well as the targeted property. For structural considerations, relativistic effects on TM atoms can have a strong impact: neglecting them for rhenium in bimetallic chloride molecules leads to an overestimation of more than 0.2 Å of Re–Re bonds.[1] On the contrary, in most cases, geometry optimizations using quantum relativistic methods of chemical systems that contain 3d elements hardly modify optimized geometries using a non-relativistic approach. Such a claim is not so straightforward for 4d transition elements: optimizing the geometry of the tetrahedral cluster $Rh_4(CO)_{12}$ using a relativistic formalism leads to a significant lengthening of Rh–Rh and Rh–C distances compared to non-relativistic optimized distances, whereas it has almost no effect on the octahedral Mo_6Br_{14} cluster although molybdenum has only three electrons less than rhodium.[2,3]

Nuclear Magnetic Resonance (NMR) is extensively used as a practical tool in chemical and materials science. Acquisition of TM-NMR spectra is not always straightforward because most of the TM nuclei have one or more unfavourable features such as a low gyromagnetic ratio and low natural abundance. The use of solid-state molybdenum NMR is hindered by these unfavourable features as well as by the quadrupolar nature of its active NMR isotopes, ^{95}Mo and ^{97}Mo. These problems can now be overcome by the use of specific pulse schemes, magic angle spinning (MAS)[4] and the development of high-magnetic-field spectrometers. ^{95}Mo NMR spectroscopy has been successfully used in the field of organometallic chemistry,[5–7] homogeneous and zeolite catalyses,[8–11] inorganic materials,[12–14] glass,[15–17] superconducting materials,[18] agricultural products,[19] *etc.* Because of its lower quadrupolar moment, the ^{95}Mo nucleus is generally preferred to ^{97}Mo.

Quantum chemical calculations of NMR parameters are important to help with interpretation of experimental data and make predictions. Among the first-principles methods, density functional theory (DFT) holds a specific place as it became the

[a] *Sciences Chimiques de Rennes, UMR 6226, CNRS - Ecole Nationale Supérieure de Chimie de Rennes, Avenue du Général Leclerc, CS 50837, 35708 Rennes cedex 7, France. E-mail: rgautier@ensc-rennes.fr; Fax: +33 2 2323 8122; Tel: +33 2 2323 8122*
[b] *Department of Physics & Astronomy, University College London, Gower Street, London WC1E 6BT, UK*

† Electronic supplementary information (ESI) available: All numerical values of NMR parameters reported in tables and ^{95}Mo NMR parameters computed for a $Mo(CO)_6$ molecule extracted from the DFT-optimized crystal structure. See DOI: 10.1039/c1cp22289a

‡ Present address: Department of Chemistry and Applied Biochemistry, ETH-Zurich, USI-Campus, Via Giuseppe Buffi 13, 6900 Lugano, Switzerland.

most popular electronic structure method owing to the accuracy that can be achieved at low computational cost. The inclusion of relativistic effects is mandatory in the calculation of NMR properties of the heaviest nuclei. Because fully relativistic four-component computations cannot be routinely handled for large chemical systems, relativistic effects can be tackled using different approaches within DFT. Most methods are based on one- or two-component formulations of the wavefunctions, with different additional approximations. Scalar relativistic (SR) effects are often introduced by the use of the Douglas–Kroll–Hess method[20,21] or the zero-order regular approximation (ZORA)[22–24] that are both two-component relativistic methods. The ZORA approach allows the variational inclusion of spin–orbit (SO) coupling.

In a recent review on DFT computations of TM-NMR parameters, even if Bühl and Kaup mentioned that chemical shift of 3d TM benefits from the use of hybrid functionals, and those of the third-row require scalar relativistic corrections, they concluded that no universal recipe for the best computational details can be given.[25] Therefore a preliminary computational study has to be achieved for each specific TM nucleus in order to determine the most appropriate computational details. This is especially true for 4d TM nuclei.

Few theoretical studies have been devoted to the DFT calculations of ^{95}Mo NMR parameters.[26–31] None of them systematically examined the influence of the main computational parameters—exchange–correlation (XC) functional, basis set, treatment of relativity, environment—on both quadrupolar interaction and chemical shift ^{95}Mo parameters. We present such a study for the molybdenum hexacarbonyl complex. A previous single-crystal ^{95}Mo solid-state NMR study at high magnetic field allowed the accurate determination of quadrupolar interaction and chemical shift parameters.[32] Moreover, since molybdenum hexacarbonyl has been used as a benchmark molecule in several previous theoretical studies using different computational approaches, this broadens the scope of the present study. It is noteworthy to mention that for the first time: (i) since structural parameters often play a part in NMR computations, their influence has been examined: ^{95}Mo NMR parameters have been computed for $Mo(CO)_6$ using the geometry determined by X-ray diffraction experiments at first,[33] the influence of geometry optimization has been studied subsequently; (ii) not only DFT calculations of an isolated $Mo(CO)_6$ molecule have been carried out but also periodic DFT calculations in order to evaluate the influence of neighbouring molecules on the NMR properties.

2 Experimental details

2.1 Crystal structure of $Mo(CO)_6$

Molybdenum hexacarbonyl crystallizes in an orthorhombic cell in space group *Pnma* (no. 62).[33] Its crystal structure solved on the basis of crystal X-ray diffraction experiments shows a single position of molybdenum. Although the local symmetry of the $Mo(CO)_6$ molecule is C_s, its geometry is pseudo-octahedral in the light of the weak range of the distances and the small deviations of the angles from 90°. Mo–C distances are 2.053 Å (×2), 2.055 Å (×2), 2.062 Å and 2.065 Å; C–O distances are 1.113 Å, 1.120 Å, 1.130 Å (×2) and 1.137 Å (×2). Mo–C and C–O averaged distances are equal to 2.057 Å and 1.129 Å, respectively.

2.2 ^{95}Mo NMR data

NMR data were taken from a high magnetic field (14.1 T) study on a monocrystal by Jakobsen *et al.*,[32] where eigenvalues of both quadrupolar coupling and chemical shift tensors have been determined accurately. ^{95}Mo chemical shifts are in ppm relative to an external 2.0 M aqueous solution of Na_2MoO_4.

The quadrupolar coupling and chemical shift parameters are defined by

$$C_Q = \frac{eQV_{zz}}{h}$$

$$\eta_Q = \frac{V_{xx} - V_{yy}}{V_{zz}}$$

$$\delta_{iso} = \tfrac{1}{3}(\delta_{xx} + \delta_{yy} + \delta_{zz})$$

$$\delta_{aniso} = \delta_{zz} - \delta_{iso}$$

$$\eta_\delta = \frac{\delta_{yy} - \delta_{xx}}{\delta_{aniso}}$$

with $|V_{zz}| \geq |V_{xx}| \geq |V_{yy}|$ and $|\delta_{zz} - \delta_{iso}| \geq |\delta_{xx} - \delta_{iso}| \geq |\delta_{yy} - \delta_{iso}|$, where ($V_{xx}$, V_{yy}, V_{zz}) and (δ_{xx}, δ_{yy}, δ_{zz}) are eigenvalues of the traceless electric field gradient (EFG) and the chemical shift tensors, respectively. The quadrupolar interaction parameters, C_Q and η_Q, are named the quadrupolar coupling constant and the asymmetry parameter, respectively. δ_{iso} and δ_{aniso} are the isotropic and anisotropic chemical shifts, respectively; η_σ is the asymmetry parameter of the chemical shift. The chemical shift tensor is connected to the chemical shielding (CS) tensor *via* the general relation:

$$\delta_{ij} = -a[\sigma_{ij} - \sigma_{ref}]$$

a is a slope that is equal to unity experimentally and σ_{ref} is the isotropic shielding of a reference compound. The shielding parameters are defined by:

$$\sigma_{iso} = \tfrac{1}{3}(\sigma_{xx} + \sigma_{yy} + \sigma_{zz})$$

$$\sigma_{aniso} = \sigma_{zz} - \sigma_{iso} = -\delta_{aniso}$$

$$\eta_\sigma = \frac{\sigma_{yy} - \sigma_{xx}}{\sigma_{aniso}} = \eta_\delta$$

with $|\sigma_{zz} - \sigma_{iso}| \geq |\sigma_{xx} - \sigma_{iso}| \geq |\sigma_{yy} - \sigma_{iso}|$.

C_Q and η_Q were measured to be 89.3 ± 0.2 kHz and 0.151 ± 0.005, respectively; δ_{iso}, δ_{aniso} and η_σ were measured to be −1854 ± 1 ppm, −11.5 ± 0.2 ppm, 0.96 ± 0.03, respectively.[32]

2.3 Computational details

Molecular DFT calculations have been carried out with the ADF package, version 2009.[34] Non-relativistic (NR) and scalar relativistic (SR) calculations using a ZORA approach have been carried out.[22–24,35] The influence of spin–orbit coupling has also been tested in scalar relativistic calculations

Table 1 Main parameters involved for the US-PP generation of all used elements

Atoms	Valence states and projectors	$r_{V_{loc}}$, $r_{V_{nloc}}$, r_{aug}/bohr	V_{loc}
Mo	$4s^{P}5s^{P}4p^{2\times P}4d^{2\times P}$	2.0, 2.0, 2.0	3
O	$2s^{2\times P}2p^{2\times P}$	1.0, 1.3, 0.7	2
C	$2s^{2\times P}2p^{2\times P}$	1.4, 1.4, 1.3	2

(SR + SO).[36] Several basis-sets included in the ADF package that are based on Slater functions have been used. The TZP-FC3d one contains triple-ζ basis sets and one polarization function for all atoms and makes use of the frozen-core approximation to treat the core electrons of Mo (1s–3d), O (1s) and C (1s).[37] The TZP and TZ2P ones are all-electron triple-ζ basis sets including one and two polarization functions for all atoms, respectively. The QZ4P is an all-electron quadruple-ζ basis set with four polarization functions for all atoms. This latter is only available for relativistic calculations. The following exchange–correlation functionals were used and compared: the local density approximation (LDA) with Vosko–Wilk–Nusair (VWN) correlation functional,[38] the BP86[39,40] and PBE[41] (generalized gradient approximation, GGA) functionals, and the B3LYP[42] and PBE0[43] hybrid functionals. EFG calculations are described in ref. 44. A quadrupolar moment Q for ^{95}Mo equal to −22 mb was used.[45,46] The ADF numerical integration factor was set to 6 in all cases. Magnetic shielding tensors have been computed with the nowadays most commonly used gauge-including atomic orbitals (GIAO) method.[47,48] CS parameters have not been computed using hybrid functionals combined with QZ4P basis sets because the needed computational facilities for such large calculations were not available.

Periodic DFT calculations were carried out with the CASTEP 4.3 code using PBE functional.[41,49,50] EFG and CS parameters were computed using PAW[51] and GIPAW[52] methods, respectively. All calculations were proven to converge in NMR values with a cutoff energy of 700 eV and a 4 × 4 × 6 *k-point* grid.[53] All ultra-soft pseudopotentials (US-PP) were generated using the OTF_ultrasoft pseudo-potential generator included in CASTEP 4.3. Relativistic effects were included for all elements during the US-PP generation by solving the scalar relativistic equation of Koelling and Harmon.[54] Most of the scalar relativistic effects acting on core electrons are included in the US-PP and on valence electrons through the interaction with the US-PP. Then, no additional calculation is needed. Spin–orbit coupling effects were not taken into account. Non-linear core corrections have been applied to all atoms.[55] US-PP parameters are given in Table 1. During geometry optimizations, only atomic positions have been relaxed. Calculations using a cubic supercell have also been carried out for a single $Mo(CO)_6$ complex. Although larger supercells have been considered, calculations were proven to converge in EFG and CS values with an edge of 12 Å length of the cubic cell.

3 Results and discussion

3.1 Calculations of NMR parameters using X-ray structural data

3.1.1 Quadrupolar interaction parameters. Computed values for different combinations of relativistic treatment, XC functional and basis sets are sketched in Fig. 1. C_Q values are almost an order of magnitude bigger than the experimental value. The parameter that influences the most the results is the basis set. Frozen core approximation leads to very different results from all-electron basis sets. This agrees with previous studies that showed that describing core electrons with a core potential gives for the EFG tensor large deviations from all-electron results.[56,57] SR treatment steadily shifts C_Q values computed using all-electron basis sets by *ca.* 40 kHz whereas SO coupling hardly modifies C_Q. This is not as important as observed by Bryce and Wasylishen for the piano-stool compound mesitylenetricarbonylmolybdenum(0).[29] However, the authors attributed to the relativistic effects the difference between a non-relativistic B3LYP calculation using a LANL2DZ basis set with a ZORA calculation using BP86 GGA functional and an all-electron triple-ζ basis set. This is not rigorous since several parameters differ in these two calculations all the more so since LANL2DZ basis used an effective core potential instead of inner core electrons. The comparison of TZP and TZ2P results shows that the effect of the additional polarization function is poorly significant. When a relativistic treatment is applied, C_Q computed with QZ4P is *ca.* 20 kHz bigger than the one computed with all-electron triple-ζ basis sets. This demonstrates that convergence of the C_Q parameter is not fully achieved towards the basis set. It is an acknowledged fact that a difference lower than 10% between experimental and computed C_Q values is satisfactory for TM solid-state NMR. Since quadrupolar coupling constants of such nuclei are often in the region of the MHz or higher, the allowed

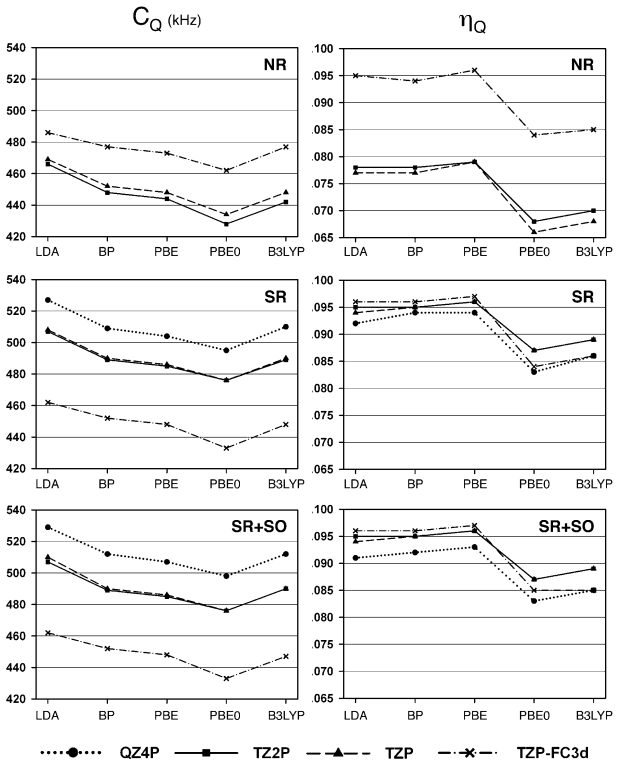

Fig. 1 ^{95}Mo quadrupolar parameters computed for $Mo(CO)_6$ using its experimental structural parameters obtained within non-relativistic (NR), scalar relativistic (SR) and scalar relativistic including spin–orbit (SR + SO) approaches.

difference is at least equal to 100 kHz. In this context, the 20 kHz difference computed between triple-ζ and quadruple-ζ basis sets appears trifling. Whatever the basis set and the relativistic treatment are, the relative order of C_Q calculated with the five different XC functionals is always the same: LDA > BP > PBE $\simeq$ B3LYP > PBE0. Since all computed values are far from the experimental one, it is not relevant to compare efficiencies of XC functionals.

All computed values of the asymmetry parameters are close to the experimental one. As regards to the XC functional, η_Q calculated with hybrid functionals are slightly lower than others. Including relativistic effects shifts η_Q values computed with all-electron basis sets by *ca.* 0.02; this leads to values between 0.08 and 0.10 that fall in the range of $\pm$0.1 usually allowed for this parameter.

PBE PAW calculations have been carried out for an isolated complex using the supercell approach. Computed C_Q and η_Q values are equal to 507 kHz and 0.10, respectively, that are rather close to the values obtained using a QZ4P basis set, the same PBE functional and a SR Hamiltonian using ADF. This tends to prove that SR US-PP takes into account most of the scalar relativistic effects in the case of molybdenum. Quadrupolar parameters have also been calculated using the crystal structure of $Mo(CO)_6$; C_Q and η_Q values are equal to 622 kHz and 0.25, respectively. The influence of neighbouring molecular units on the calculation of these quadrupolar parameters is significant, even if molybdenum hexacarbonyl is a molecular crystal, weaker but significant interactions occur between molecular units. In a way, this partly casts doubt over the molecular approach for the calculation of the quadrupolar parameters that consists in approximating the periodic structure of a compound as a 'molecule'.[58–62]

3.1.2 Chemical shielding parameters. First-principles calculations of ^{95}Mo CS parameters of molybdenum hexacarbonyl have already been the subject of few studies.[26–28,30] Most of them use a relativistic approach of shielding calculations.[26,28,30] Schreckenbach and Ziegler used a quasi-relativistic method employing a Pauli-type Hamiltonian to compute ^{17}O and metal CS parameters of some $[MO_4]^{n-}$ (M = Cr, Mo, W, Mn, Tc, Re, Ru, Os) complexes and group 6 hexacarbonyls. Later, Baerends *et al.* published a study using the two-component relativistic method, ZORA, that enables the use of all-electron basis sets and thus improves the computed isotropic shielding values for the same TM series. These two studies were carried out on experimental geometries and make use of the BP86 functional.[39,40] None of them report anisotropic and asymmetry CS parameters. Recently, Filatov and Cremer reported ^{95}Mo and ^{183}W shielding isotropic parameters computed using a quasi-relativistic approach within the normalized elimination of the small component approximation combined with "independent gauge for localized orbitals" (IGLO) DFT method.[30] In the latter study, calculations have been carried out on an idealized octahedral geometry of molybdenum hexacarbonyl with Mo–C and C–O bond distances equal to 2.063 Å and 1.145 Å respectively. The effect of SO coupling has not been investigated in all these studies.

^{95}Mo CS results are sketched in Fig. 2. As previously reported by Baerends *et al.*,[28] the frozen core approximation

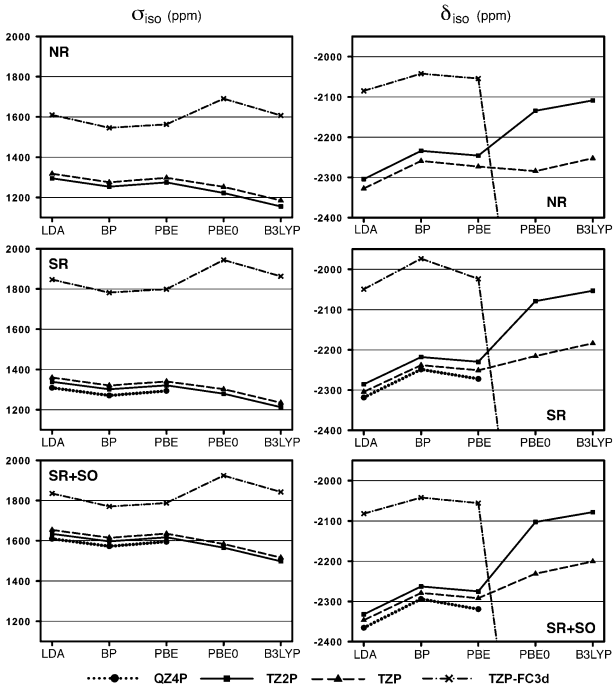

Fig. 2 ^{95}Mo σ_{iso} and δ_{iso} computed for $Mo(CO)_6$ using its experimental structural parameters obtained within non-relativistic (NR), scalar relativistic (SR) and scalar relativistic including spin–orbit (SR + SO) approaches. Isotropic chemical shielding computed using a TZP-FC3d basis set and hybrids are missing because they range between −3050 and −3145 ppm.

strongly affects the computed σ_{iso} whatever the XC functional and the relativistic treatments are. The most important difference occurs when SR calculations were carried out. Using that basis set, GGA computed values are roughly 50 ppm lower than LDA values. σ_{iso} computed with PBE0 and B3LYP functionals are *ca.* 150 and 50 ppm, respectively, bigger than GGA values. Whatever the relativistic treatment is, all-electron isotropic CS values have the same behaviour with respect to XC functional. For the same XC functional and relativistic treatment, σ_{iso} computed with TZP, TZ2P and QZ4P lie within 50 ppm at the most. Although this value might seem large, it is not that much regard to the experimental ^{95}Mo δ_{iso} range in the solid-state that is almost equal to 8000 ppm. Whatever the relativistic treatment and the all-electron basis set are, the relative order of σ_{iso} calculated with the five different XC functionals is always the same: LDA > PBE > BP $\simeq$ PBE0 > B3LYP. Considering the same all-electron basis set, LDA, GGA and PBE0 computed σ_{iso} lie within less than 50 ppm. B3LYP σ_{iso} is *ca.* 70 ppm lower than PBE0 values. Filatov and Cremer also noticed that B3LYP-computed σ_{iso} values are lower than BLYP-computed ones.[30] As suggested by Reiher *et al.*,[63] the 20% amount of Hartree–Fock exchange in B3LYP may be at the origin of this behaviour and should be reduced to 15% for a better description of TM compounds. GIPAW computed σ_{iso} on the isolated $Mo(CO)_6$ and its crystal structure are equal to 1340 and 1277 ppm, respectively. The former is rather close to the ones obtained with ADF using all-electron triple-ζ basis sets, PBE functional and scalar relativistic calculations. The difference

of 63 ppm between GIPAW computed σ_{iso} using both approaches shows that neighbouring molecules in the crystal play a part.

One of the most striking features is the effect of spin–orbit coupling on the computed isotropic CS parameter: NR and SR computed σ_{iso} are in the region of 1150–1350 ppm whereas σ_{iso} computed considering SR + SO corrections are in the region of 1500–1650 ppm. Such a large SO effect has been observed for ^{99}Ru and ^{103}Rh nuclei in a wide variety of complexes.[64,65] Several theoretical studies showed that SO effects are more important for the shifts of nuclei bonded to a heavy atom than for those of the heavy nuclei themselves.[25] Moreover, it has been reported that even if relativistic effects can be important on σ_{iso} of 4d nuclei, they almost cancel for computed isotropic chemical shifts since relativistic shielding terms are weakly sensitive to the chemical surroundings of the heavy atom. Chemical shifts relative to the experimental standard, $[MoO_4]^{2-}$, have been estimated by computing isotropic ^{95}Mo CS parameters of the tetraoxo dianion using the same basis set, XC functional and relativistic treatment. Results are sketched in Fig. 2. The frozen core approximation leads to different isotropic ^{95}Mo chemical shifts than all-electron basis sets. Baerends *et al*. also mentioned this result.[28] Using all-electron basis sets, isotropic chemical shifts are more deshielded than the experimental one, ranging from −2100 to −2300 ppm. Bühl observed the same trend for several organometallic complexes and inorganic ions.[27] LDA and GGA computed values are rather close whatever the all-electron basis set is. Using hybrid functionals, TZ2P δ_{iso} are *ca*. 50 ppm more deshielded than TZP ones. The frozen core basis set combined with hybrid functionals leads to ^{95}Mo isotropic chemical shift computed below −3000 ppm. This arises from isotropic CS values computed for the $[MoO_4]^{2-}$ that are surprisingly very deshielded. There is a significant basis effect on δ_{iso} computed using hybrid functionals since the difference between TZP and TZ2P values can reach *ca*. 150 ppm. Since this effect is not visible for the corresponding σ_{iso}, this can be attributed to the computation of σ_{iso} of the reference compound $[MoO_4]^{2-}$ where a large basis set is required for a good description of the double anionic charge. This might be related to the Hartree–Fock exchange of hybrids that require extended basis sets for reliable densities.[66,67] The additional function in the TZ2P basis set gives the flexibility needed for the tetraoxo anion. To go further, it would be instructive to compute σ_{iso} using QZ4P basis sets and hybrid functionals.

The influence of relativistic treatment on ^{95}Mo isotropic chemical shift slightly varies according to the XC functional and the basis set. Using all-electron basis sets, SR corrections shift LDA and GGA δ_{iso} by *ca*. −20 ppm whereas they shift hybrid XC computed δ_{iso} by about −65 ppm. Including SO effects in all-electron calculations shields LDA and GGA ^{95}Mo δ_{iso} by about +45 ppm and hybrid ^{95}Mo δ_{iso} by about +20 ppm. Using the frozen-core approximation leads to close NR and SR + SO isotropic chemical shifts. In the light of computed σ_{iso}, this indicates that the shift of the isotropic CS computed when relativistic effects are considered is of the same order of magnitude for $Mo(CO)_6$ and $[MoO_4]^{2-}$ as well. From a chemical point of view, these units are rather different: the oxidation state of molybdenum is zero in $Mo(CO)_6$ whereas it is +VI in the dianion. In both chemical species, only core electrons must behave similarly. Then, since relativistic effects shift similarly ^{95}Mo σ_{iso} of $Mo(CO)_6$ and $[MoO_4]^{2-}$, valence electrons must be more affected by relativity than core ones.

The computed ^{95}Mo anisotropic CS parameters sketched in Fig. 3 follow the same trend for each relativistic treatment. Using the frozen core basis set to compute ^{95}Mo δ_{aniso} leads to values close to the one obtained with all-electron basis sets. The influence of XC functional is more noteworthy. LDA δ_{aniso} range from 3 to 5 ppm. BP and PBE δ_{aniso} shift *ca*. −1 ppm and −0.8 ppm, respectively. A systematic negative shift also occurs when hybrid XC functionals are used: Computed δ_{aniso} range between 0.9 and 1.7 ppm. These computed values are rather far from the experimental ones that vary from −11 to −12.5 ppm.[32] Relativistic corrections hardly change δ_{aniso}. GIPAW computed δ_{aniso} is equal to −5.17 ppm for the isolated $Mo(CO)_6$ whereas it is −15.61 ppm for the crystal structure. This shows that surrounding molecules in the crystal have a strong influence on this anisotropic chemical shift parameter. Since computed δ_{aniso} values are far from the measured one, one cannot expect any agreement between calculated and measured η_σ. Asymmetry parameters of the ^{95}Mo CS are shown in Fig. 3. All LDA values are in the region of 0.40 whereas GGA ones lie between 0.45 and 0.70. Convergence with respect to the basis set is almost achieved using these functionals. Conversely, η_σ computed using hybrid functionals can be very different according to the basis set and the relativistic treatment. Although some of these latter are close to the experimental one, *i. e*. 0.96, this agreement must be considered as a matter of chance. GIPAW η_σ computed within the supercell approach and considering the $Mo(CO)_6$ crystal

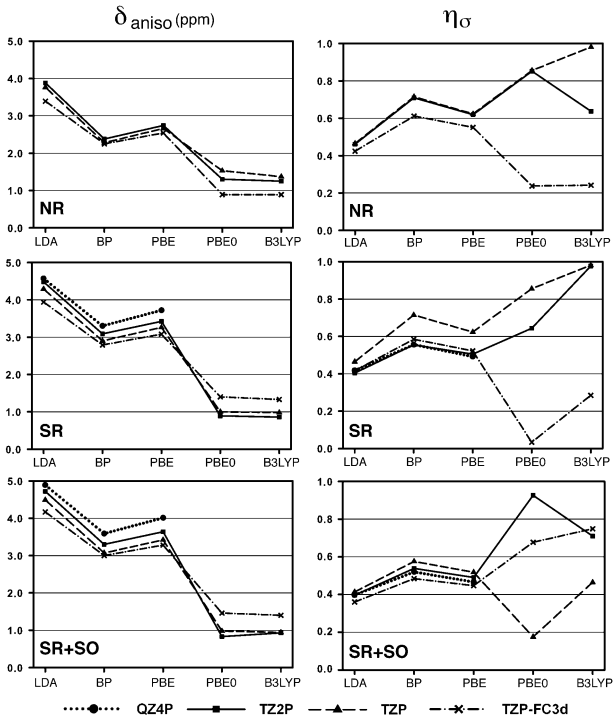

Fig. 3 ^{95}Mo δ_{aniso} and η_σ computed for $Mo(CO)_6$ using its experimental structural parameters obtained within non-relativistic (NR), scalar relativistic (SR) and scalar relativistic including spin–orbit (SR + SO) approaches

structure are equal to 0.51 and 0.65, respectively. These values are rather close to the one computed for the isolated complex using PBE, but also far from the experimental value.

3.2 Geometry optimizations

There are two types of relativistic effects on the NMR parameters: changes in the NMR parameters due to relativistic changes in the geometries, in particular the relativistic bond contraction,[68] and direct relativistic effects at a given geometry. While the latter has been studied in the previous section, the former has to be estimated as well as the influence of XC functional and basis sets. Therefore, geometry optimizations have been carried out. Since we intend to study the influence of basis sets, XC functional as well as relativistic corrections as in the previous section, geometry optimizations have been both carried out on a single $Mo(CO)_6$ molecule using ADF and CASTEP (with the supercell approach) programs and by considering the crystallographic structure using CASTEP. Optimizing the geometry of an isolated $Mo(CO)_6$ complex leads to an ideal octahedral unit. This proves that the C_s geometry of the organometallic complex in the crystal is due to crystal packing effects. Mo–C and C–O optimized distances are sketched in Fig. 4. One of the most striking features of Fig. 4 is the weak influence of structural parameters of $Mo(CO)_6$ towards relativistic formalism. Moreover SR and SO + SR optimized distances are nearly equal. Although few theoretical studies were devoted to $Mo(CO)_6$,[69–74] none of them mentioned this behavior for relaxed geometries. A recent study showed that relativistic effects on ionization energies of $Mo(CO)_6$ are also negligible.[74]

LDA functional underestimates Mo–C optimized distances compared to X-ray ones. This is consistent with the overestimation of binding energies of LDA functionals.[75] Non-relativistic GGA optimized Mo–C and C–O distances are *ca.* 0.03 Å and 0.01 Å, respectively, longer than LDA distances. SR GGA optimizations lead to shorter Mo–C distances that are very close to the experimental one; the average experimental Mo–C distance being equal to 2.057 Å. C–O optimized bond distances are about 0.025 Å longer than the averaged experimental one equal to 1.129 Å. Such an overestimation is also observed in the previous GGA-DFT studies on this complex.[70] Using hybrid functionals partly corrects the optimized C–O distance by about 0.015 Å. Combined with the use of the most extended basis set, the averaged C–O bond is computed to 1.139 Å and 1.137 Å using B3LYP and PBE0 functionals, respectively. Such an agreement between both hybrid functionals is not observed for Mo–C bonds: PBE0 optimized distances are close to other GGA values and the averaged experimental one whereas B3LYP can exceed 2.10 Å using the frozen core basis set. Although this overestimation is softened using more extended basis set, Mo–C bonds optimized using B3LYP exceed 2.08 Å whatever the basis set and the relativistic treatment are.

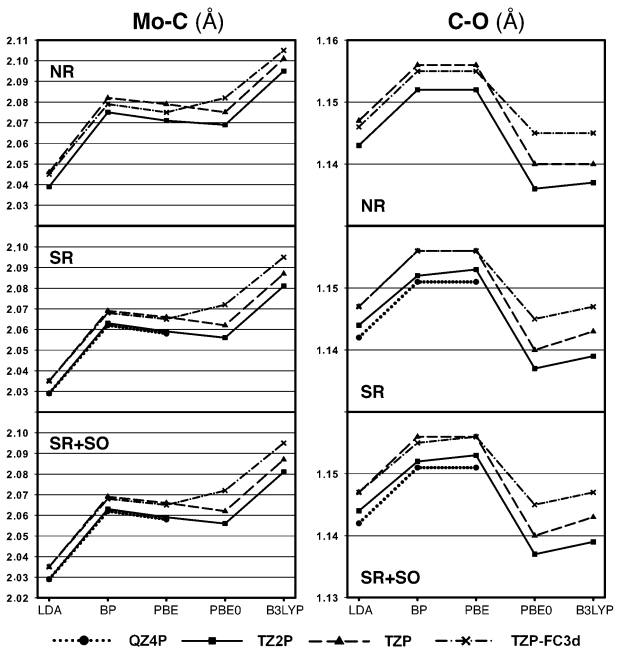

Fig. 4 Mo–C and C–O distances of $Mo(CO)_6$ optimized within non-relativistic (NR), scalar relativistic (SR) and scalar relativistic including spin–orbit (SR + SO) approaches.

The supercell technique has also been used to optimize the geometry of an isolated $Mo(CO)_6$ motif with CASTEP using PBE functional. The optimized geometry is octahedral and Mo–C and C–O bond distances are equal to 2.055 Å and 1.156 Å, respectively. These distances are close to the one obtained using the ADF program and the same XC functional and SR formalism. Mo–C distances resulting from crystal structure optimization vary from 2.046 Å to 2.051 Å. This is approximately 0.01 Å shorter than SR-PBE optimized distances for the isolated complex. This small discrepancy can be due to crystal packing effects. Freezing cell parameters during the geometry optimization may also have an impact on the result. However, since neither LDA nor GGA deals very well with long distance interactions, relaxing cell parameters leads to excessively large values of the cell parameters.

3.3 Calculations of NMR parameters using optimized geometries

In the previous section, we have shown that optimizing the geometry of an isolated $Mo(CO)_6$ molecule leads to an octahedral chemical species. Such a high symmetry nullifies the quadrupolar interaction parameters as well as anisotropic and asymmetry CS parameters of the central molybdenum atom. Although optimized bonds and angles are not very far from the one resulting from X-ray diffraction studies, it turns out that NMR parameters are very sensitive towards geometrical variables. The combined influence of computational and structural parameters can still be studied for the isotropic chemical shielding and shift, whose values are reported in Fig. 5. These latter were obtained for the geometry-optimized octahedral units using the same computational details for both geometry optimization and NMR calculation.

Optimizing the geometry of $Mo(CO)_6$ leads to some shift of the isotropic CS compared to the corresponding values obtained using the same computational details. While TZP-FC3d/LDA values remain almost the same, TZP-FC3d/GGA σ_{iso} are computed *ca.* 100 ppm lower. This shift is more important using hybrids with a frozen-core basis set, the largest occurring

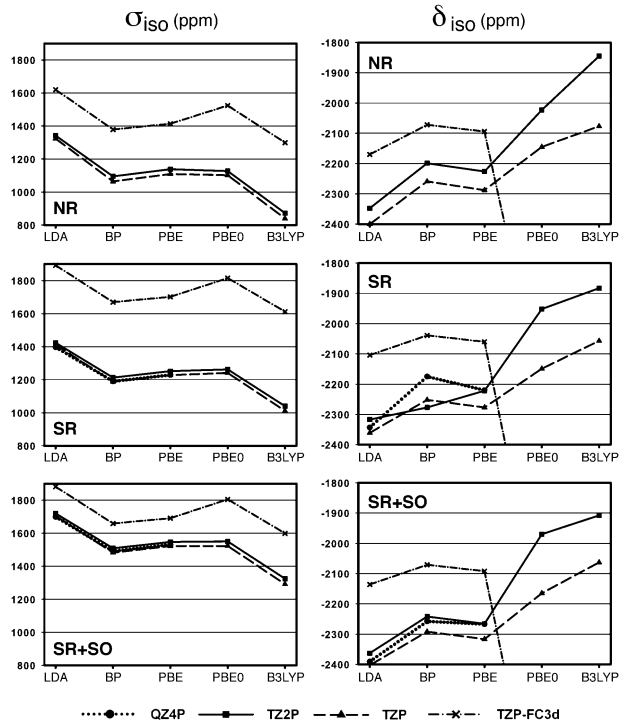

Fig. 5 ^{95}Mo σ_{iso} and δ_{iso} computed for $Mo(CO)_6$ optimized geometries obtained within non-relativistic (NR), scalar relativistic (SR) and scalar relativistic including spin–orbit (SR + SO) approaches. Isotropic chemical shielding computed using a TZP-FC3d basis set and hybrids are missing because they range between −2920 and −3009 ppm.

using B3LYP. These shifts hardly depend upon the relativistic formalism. Using all-electron basis sets and without relativistic effects, GGA and PBE0 σ_{iso} are also shifted by *ca.* −150/200 ppm whereas B3LYP values are lower than 900 ppm, that is about 300 ppm lower than the one computed for the experimental geometry using the same functional. Within a series of σ_{iso} computed using the same basis set, it is interesting to mention that the shorter the optimized Mo–C bond, the larger the isotropic CS. Furthermore, differences of σ_{iso} values computed using all-electron basis sets and the same XC functional are about 20 ppm: when relativistic effects are taken into account, QZ4P σ_{iso} are nearly equal to TZP values whereas TZ2P σ_{iso} are a bit larger.

Chemical shifts have been estimated by computing isotropic ^{95}Mo CS parameters for optimized geometries of $[MoO_4]^{2-}$ using the same basis set, XC functional and relativistic treatment. As observed in the previous section, ^{95}Mo δ_{iso} computed using a frozen core basis set and hybrid functionals are below −2900 ppm; this is due to unexplained extremely deshielded σ_{iso} of $[MoO_4]^{2-}$ units using these computational details. In comparison with calculations carried out for the X-ray geometry on an isolated $Mo(CO)_6$ complex, σ_{iso} computed using frozen-core basis sets are between −50 to −150 ppm shielded. For all-electron LDA and GGA calculations, the variations are rather slight and rarely exceed ±50 ppm; ^{95}Mo δ_{iso} range between −2175 and −2400 ppm that is rather far from the experimental signal that resonates at −1854 ppm. Using hybrids and all-electron basis sets, and considering optimized geometries using the same computational details, ^{95}Mo δ_{iso} are more shielded than the other all-electron values for optimized geometries whatever the relativistic treatment is considered. Moreover, TZ2P ^{95}Mo δ_{iso} are more deshielded than TZP values, and B3LYP δ_{iso} are more deshielded than PBE0. TZ2P-B3LYP ^{95}Mo δ_{iso} range between −1908 and −1845 ppm depending upon relativistic treatment. This result does not follow the trend previously observed that GGA better reproduce isotropic CS than hybrids:[27] PW91 and B3LYP δ_{iso} were computed to −2294 ppm and −2350 ppm, respectively. However, these values were obtained using computed ^{95}Mo σ_{iso} of −1358 and −1192 ppm for $[MoO_4]^{2-}$ using B3LYP and PW91, respectively. These reference values are far more shielded than the one we obtained using GGA and B3LYP functionals. This probably comes from the Mo–O bond distance of 1.809 Å that has been considered in the previous study, which is largely overestimated as shown by the optimized Mo–O distance of 1.764 Å also mentioned in this study. As for the calculations carried out on the X-ray geometry of $Mo(CO)_6$, there is a strong basis effect on δ_{iso} computed using hybrid functional: difference between TZP and TZ2P values can reach 250 ppm.

The GIPAW supercell calculation gives results similar to GIAO molecular calculations using PBE and a scalar relativistic treatment, σ_{iso} is computed to be equal to 1279 ppm. GIPAW calculations considering the optimized crystal structure lead to a close σ_{iso} value of 1245 ppm. However, since optimizing the crystal structure does not lead to idealized octahedral $Mo(CO)_6$, anisotropic and asymmetry CS parameters as well as EFG parameters are non-zero. For this optimized crystal structure, δ_{aniso} and η_σ are equal to −11.89 ppm and 0.96, respectively. These values are in very good agreement with the experimental one. Moreover, quadrupolar interaction parameters, C_Q and η_Q, are equal to 100 kHz and 0.68, respectively. The agreement between experiment and computation is excellent for the quadrupolar coupling constant equal to 89 kHz. Conversely, the difference between experimental and computed η_Q is large.

The effect of environment on the geometry optimization is obvious in the case of $Mo(CO)_6$. In order to evaluate the ability of a molecular approach to compute ^{95}Mo NMR parameters of $Mo(CO)_6$, calculations have been carried out on a single complex extracted from the optimized crystal structure of molybdenum hexacarbonyl. EFG and CS parameters have been computed using this "benchmark" optimized geometry and various basis sets, XC functionals and relativistic treatments. Complete ^{95}Mo NMR parameters are provided in the ESI.† Whatever the computational details are, the computed quadrupolar coupling constant ranges between 140 and 180 kHz, whereas most of the computed η_Q lie around 0.4. For C_Q, considering an optimized geometry improves the agreement with experiment. In contrast, the computed asymmetry parameters deviate from the experimental value. This can be explained by the small EFG eigenvalues that are particularly sensitive to weak structural variations. For isotropic shielding and shift parameters, curves look like the one obtained for the X-ray geometry: σ_{iso} values obtained using the same computational details are shifted by less than 50 ppm. A shift of +50 ppm then follows for the δ_{iso} curves. δ_{aniso} range between −1.5 and −3.5 ppm. Even if computing properly the sign of this parameter is an improvement compared

to the calculations based on the X-ray geometry, it is still far from the experimental value. Moreover, this computed anisotropic parameter roughly behaves as the one calculated for the X-ray geometry. This is not the case for the asymmetry CS parameters that range between 0.2 and 0.8.

4 Conclusions

We have given in this contribution a complete benchmark study of the molecular DFT computations of ^{95}Mo NMR parameters of molybdenum hexacarbonyl. Both quadrupolar interaction and chemical shielding parameters have been computed while varying XC functional, basis sets and relativistic corrections. Results were compared with periodic DFT calculations for the isolated $Mo(CO)_6$ molecule as well as the solid state compound.

The DFT molecular study shows that structural parameters prevail over computational details to calculate EFG parameters, in particular the quadrupolar coupling constant. For a fixed-geometry complex, the molecular computed asymmetry parameter of the quadrupolar interaction is converged with respect to the computational parameters. This is not clear for the quadrupolar coupling constant, even if the largest difference between all computed values for the experimental geometry is equal to 100 kHz, that is rather low with respect to the usual accuracy of solid-state NMR experiments. Relativistic effects have a minor influence on the computations of ^{95}Mo quadrupolar interaction parameters. The molecular approach fails to compute the quadrupolar coupling constant of molybdenum hexacarbonyl. First, geometry optimizations of the $Mo(CO)_6$ complex lead to highly symmetrical units for which EFG parameters are zero. This proves that geometry optimization must be handled carefully in that case. Moreover, even if a geometry extracted from an optimized crystal structure is considered for a molecular EFG calculation, the computed value still deviates from periodic EFG calculations, particularly the asymmetry parameter. Our study shows that periodic EFG calculations must be preferred to molecular calculations, at least for the quadrupolar coupling constant, even for the study of inorganic molecular compounds.

Isotropic chemical shift and shielding are more sensitive to computational details. As already mentioned in the literature,[28] basis sets effects are important. In particular, the frozen core approximation strongly affects the isotropic CS and to a lesser extent the isotropic chemical shift. However, the difference between δ_{iso} computed within the frozen core approximation and using all-electron basis sets can reach 200 ppm. δ_{iso} is less sensitive to the relativistic treatments than σ_{iso}. In particular, SO effects are important for σ_{iso} but cancel for δ_{iso}: Core electrons are the most affected by relativistic effects and since core orbitals are quite invariant to the chemical surroundings, only small chemical shift effects arise from relativity. Finally, hybrid functionals perform better than LDA and GGA functionals for the computations of these isotropic parameters: B3LYP combined with the most extended all-electron triple-ζ basis set leads to δ_{iso} equal to -1883 ppm for the optimized geometry; the experimental value is -1854 ppm. The choice of XC functional also plays an important part in the computations of δ_{aniso} and η_σ. These parameters are also sensitive to the basis set and relativistic treatment as well as structural parameters. Within the molecular approach, it seemed difficult to get any agreement for the anisotropic and asymmetry CS parameters with experimental values.

Our study showed that it is difficult to get reliable ^{95}Mo NMR parameters within a molecular approach, perhaps with the exception of the isotropic CS and chemical shift. Since the calculations carried out within the supercell approach using periodic boundary conditions give results similar to the one obtained using a molecular approach and carried out with analogous computational details, this proves that it must be attributed to the molecular approach rather than a failure of the ADF program. ^{95}Mo solid-state NMR parameters can be reproduced well by the use of the PAW and GIPAW methods and the crystal structure of molybdenum hexacarbonyl. Although it is an organometallic molecular compound, ^{95}Mo NMR parameters of molybdenum hexacarbonyl are highly influenced by its crystal structure. Geometry optimization is mandatory to get reliable NMR parameters within the periodic approach. In order to take into account relativistic effects, the use of relativistic pseudo potentials in the PAW approach is enough relevant for the computations of ^{95}Mo NMR parameters.

Acknowledgements

We thank Dr Hans Martin Senn for helpful discussions. RG and LLP are indebted to the Région Bretagne for a PhD grant (JC). LLP thanks Rennes Metropole for a grant. This work was granted access to the HPC resources of CINES under the allocation 2009-086170 made by GENCI (Grand Equipement National de Calcul Intensif). The authors acknowledge the support of the French Agence Nationale de la Recherche (ANR), under grant NMRTHEO (ANR-09-JCJC-0088-01).

References

1 S. Petric and R. Stranger, *Inorg. Chem.*, 2004, **43**, 2597.
2 K. Besanon, G. Laurenczy, T. Lumini, R. Roulet, R. Bruyndonckx and C. Daul, *Inorg. Chem.*, 1998, **37**, 5634.
3 K. Kirakci, S. Cordier, A. Shames, B. Fontaine, O. Hernandez, E. Furet, J.-F. Halet, R. Gautier and C. Perrin, *Chem.–Eur. J.*, 2007, **13**, 9608–9616.
4 E. R. Andrew, *Prog. Nucl. Magn. Reson. Spectrosc.*, 1971, **8**, 1–39.
5 M. N. Ackermann, K. B. Moore, A. S. Colligan, J. A. Thomas-Wohlever and K. J. Warren, *J. Organomet. Chem.*, 2003, **667**, 81–89.
6 J. A. Brito, H. Teruel, S. Massoud and M. Gomez, *Magn. Reson. Chem.*, 2009, **47**, 573–577.
7 R. A. Lal, M. Chakrabarty, S. Choudhury, A. Ahmed, R. Borthakur and A. Kumar, *J. Coord. Chem.*, 2010, **63**, 163–175.
8 H. Zheng, D. Ma, X. Bao, J. Z. Hu, J. H. Kwak, Y. Wang and C. H. F. Peden, *J. Am. Chem. Soc.*, 2008, **130**, 3722–3723.
9 J. Z. Hu, J. H. Kwak, Y. Wang, C. H. F. Peden, H. Zheng, D. Ma and X. Bao, *J. Phys. Chem. C*, 2009, **113**, 2936–2942.
10 D. Ren, X. Wang, G. Li, X. Cheng, H. Long and L. Chen, *J. Nat. Gas Chem.*, 2010, **19**, 646–652.
11 H. J. Jakobsen, H. Bildsoe, J. Skibsted, M. Brorson and K. Schaumburg, *Chem. Commun.*, 2010, **46**, 2103–2105.
12 L. Kazansky and B. McGarvey, *Coord. Chem. Rev.*, 1999, **188**, 157–210.
13 L. Kazansky and T. Yamase, *J. Phys. Chem. A*, 2004, **108**, 6437–6448.
14 M. A. M. Forgeron and R. E. Wasylishen, *J. Am. Chem. Soc.*, 2006, **128**, 7817–7827.

15 N. Machida and H. Eckert, *Solid State Ionics*, 1998, **107**, 255–268.
16 S. H. Santagneli, C. C. de Araujo, W. Strojek, H. Eckert, G. Poirier, S. J. L. Ribeiro and Y. Messaddeq, *J. Phys. Chem. B*, 2007, **111**, 10109–10117.
17 S. Kroeker, I. Farnan, S. Schuller and T. Advocat, *Scientific Basis for Nuclear Waste Management XXXII*, 2009, pp. 153–159.
18 L. Le Pollès, R. Gautier, J. C. Ameline, M. Le Floch and O. Peña, *Solid State Commun.*, 2003, **125**, 597–600.
19 D. R. Steinke, W. Majak, T. S. Sorensen and M. Parvez, *J. Agric. Food Chem.*, 2008, **56**, 5437–5442.
20 M. Douglas and N. M. Kroll, *Ann. Phys. (Leipzig)*, 1974, **82**, 89–155.
21 B. A. Hess, *Phys. Rev. A: At., Mol., Opt. Phys.*, 1986, **33**, 3742–3748.
22 E. van Lenthe, E. J. Baerends and J. G. Snijders, *J. Chem. Phys.*, 1993, **99**, 4597–4610.
23 R. van Leeuwen, E. van Lenthe, E. J. Baerends and J. G. Snijders, *J. Chem. Phys.*, 1994, **101**, 1272–1281.
24 E. van Lenthe, E. J. Baerends and J. G. Snijders, *J. Chem. Phys.*, 1994, **101**, 9783–9792.
25 M. Bühl and M. Kaupp, in *Computational Inorganic and Bioinorganic Chemistry*, ed. E. I. Solomon, R. A. Scott and R. B. King, Wiley, 2009, pp. 91–108.
26 G. Schreckenbach and T. Ziegler, *Int. J. Quantum Chem.*, 1997, **61**, 899–918.
27 M. Bühl, *Chem.–Eur. J.*, 1999, **5**, 3514–3522.
28 R. Bouten, E. J. Baerends, E. van Lenthe, L. Visscher, G. Schreckenbach and T. Ziegler, *J. Phys. Chem. A*, 2000, **104**, 5600–5611.
29 D. L. Bryce and R. E. Wasylishen, *Phys. Chem. Chem. Phys.*, 2002, **4**, 3591–3600.
30 M. Filatov and D. Cremer, *J. Chem. Phys.*, 2003, **119**, 701.
31 J. Cuny, E. Furet, R. Gautier, L. Le Polles, C. J. Pickard and J.-B. d'Espinose de Lacaillerie, *ChemPhysChem*, 2009, **10**, 3320–3329.
32 T. Vosegaard, J. Skibsted and H. Jakobsen, *J. Phys. Chem. A*, 1999, **103**, 9144–9149.
33 T. Mak, *Z. Kristallogr.*, 1984, **166**, 277–281.
34 G. te Velde, F. M. Bickelhaupt, E. J. Baerends, C. Fonseca Guerra, S. J. A. van Gisbergen, J. G. Snijders and T. Ziegler, *J. Comput. Chem.*, 2001, **22**, 931–967.
35 A. J. Sadlej, J. G. Snijders, E. van Lenthe and E. J. Baerends, *J. Chem. Phys.*, 1995, **102**, 1758–1766.
36 S. Faas, J. H. van Lenthe, A. C. Hennum and J. G. Snijders, *J. Chem. Phys.*, 2000, **113**, 4052–4059.
37 E. J. Baerends, D. E. Ellis and P. Ros, *Chem. Phys.*, 1973, **2**, 41–51.
38 S. D. Vosko, L. Wilk and M. Nusair, *Can. J. Chem.*, 1990, **58**, 1200.
39 A. G. Becke, *Phys. Rev. A: At., Mol., Opt. Phys.*, 1988, **38**, 3098.
40 J. P. Perdew, *Phys. Rev. B: Condens. Matter Mater. Phys.*, 1986, **33**, 8822.
41 J. P. Perdew, K. Burke and M. Ernzerhof, *Phys. Rev. Lett.*, 1996, **77**, 3865–3868.
42 A. D. Becke, *J. Chem. Phys.*, 1993, **98**, 1372–1377.
43 C. Adamo and V. Barone, *J. Chem. Phys.*, 1999, **110**, 6158–6170.
44 E. van Lenthe and E. J. Baerends, *J. Chem. Phys.*, 2000, **112**, 8279.
45 K. J. D. MacKenzie and M. E. Smith, *Multinuclear Solid-State NMR of Inorganic Materials*, Pergamon, 2002.
46 P. Pyykkö, *Mol. Phys.*, 2001, **99**, 1617–1629.
47 R. Ditchfield, *J. Chem. Phys.*, 1972, **56**, 5688–5691.
48 K. Wolinski, J. F. Hinton and P. Pulay, *J. Am. Chem. Soc.*, 1990, **112**, 8251–8260.
49 S. J. Clark, M. D. Segall, C. J. Pickard, P. J. Hasnip, M. J. Probert, K. Refson and M. C. Payne, *Z. Kristallogr.*, 2005, **220**, 567–570.
50 M. D. Segall, P. J. D. Lindan, M. J. Probert, C. J. Pickard, P. J. Hasnip, S. J. Clark and M. C. Payne, *J. Phys.: Condens. Matter*, 2002, **14**, 2717–2744.
51 P. E. Blöchl, *Phys. Rev. B: Condens. Matter Mater. Phys.*, 1994, **50**, 17953–17979.
52 C. J. Pickard and F. Mauri, *Phys. Rev. B: Condens. Matter Mater. Phys.*, 2001, **63**, 245101.
53 H. J. Monkhorst and J. D. Pack, *Phys. Rev. B: Condens. Matter Mater. Phys.*, 1976, **13**, 5188–5192.
54 D. D. Koelling and B. N. Harmon, *J. Phys. C: Solid State Phys.*, 1977, **10**, 3107–3114.
55 S. G. Louie, S. Froyen and M. L. Cohen, *Phys. Rev. B: Condens. Matter Mater. Phys.*, 1982, **26**, 1738–1742.
56 J. N. Latosińska, *Int. J. Quantum Chem.*, 2003, **91**, 284–296.
57 R. Bjornsson and M. Bühl, *Dalton Trans.*, 2010, 5319–5324.
58 J. A. Tossell, *Phys. Chem. Miner.*, 1999, **27**, 70.
59 M. J. Willans and R. W. Schurko, *J. Phys. Chem. B*, 2003, **107**, 5144.
60 T. M. Clark and P. J. Grandinetti, *J. Phys.: Condens. Matter*, 2003, **15**, 2387.
61 B. R. Cherry, T. M. Alam, C. Click, R. K. Brow and Z. Gan, *J. Phys. Chem. B*, 2003, **107**, 4894.
62 T. M. Clark and P. J. Grandinetti, *Solid State Nucl. Magn. Reson.*, 2005, **27**, 233–241.
63 M. Reiher, O. Salomon and B. A. Hess, *Theor. Chem. Acc.*, 2001, **107**, 48–55.
64 A. Bagno and M. Bonchio, *Magn. Reson. Chem.*, 2004, **42**, S79–S87.
65 L. Orian, A. Bisello, S. Santi, A. Ceccon and G. Saielli, *Chem.–Eur. J.*, 2004, **10**, 4029–4040.
66 B. S. Jursic, *J. Mol. Struct. (THEOCHEM)*, 1999, **467**, 1–6.
67 M.-C. Kim, E. Sim and K. Burke, *J. Chem. Phys.*, 2011, **134**, 171103.
68 P. Pyykkö, *Chem. Rev.*, 1988, **88**, 563–594.
69 A. W. Ehlers and G. Frenking, *J. Am. Chem. Soc.*, 1994, **116**, 1514.
70 A. Rosa, E. J. Baerends, S. J. A. van Gisbergen, E. van Lenthe, J. A. Groeneveld and J. G. Snijders, *J. Am. Chem. Soc.*, 1999, **121**, 10356.
71 R. Sniatynsky and D. L. Cedeno, *J. Mol. Struct. (THEOCHEM)*, 2004, **711**, 123.
72 Y. Ishikawa and K. Kawakami, *J. Phys. Chem. A*, 2007, **111**, 99540.
73 C. A. Bayse and K. N. Ortwine, *J. Phys. Chem. A*, 2007, **111**, 7841.
74 R. Fukuda, S. Hayaki and H. Nakatsuji, *J. Chem. Phys.*, 2009, **131**, 174303.
75 D. Rappoport, N. R. M. Crawford, F. Furche and K. Burke, in *Computational Inorganic and Bioinorganic Chemistry*, ed. E. I. Solomon, R. B. King and R. A. Scott, Wiley, 2009, ch. 12, p. 159.